IOSA investigations of the effects of potential surface topography upon elastic and inelastic scattering and rotational relaxation in the (He, CO2) system

P. M. Agrawal and L. M. Raff

Citation: The Journal of Chemical Physics **75**, 2163 (1981); doi: 10.1063/1.442329
View online: http://dx.doi.org/10.1063/1.442329
View Table of Contents: http://scitation.aip.org/content/aip/journal/jcp/75/5?ver=pdfcov
Published by the AIP Publishing

IOSA investigations of the effects of potential surface topography upon elastic and inelastic scattering and rotational relaxation in the (He, CO_2) system[a)]

P. M. Agrawal[b)] and L. M. Raff

Department of Chemistry, Oklahoma State University, Stillwater, Oklahoma 74078
(Received 30 June 1980; accepted 8 August 1980)

The effect of potential surface topography upon elastic and inelastic scattering has been investigated using the infinite-order sudden approximation (IOSA) to compute total differential and integral cross sections, state-to-state cross sections, and the relaxation rates of depleted levels in the (He, CO_2) and (^{3}He, CO_2) rigid rotor systems on six different potential energy surfaces that include three surfaces obtained from electrom–gas type calculations, two *ab initio* SCF surfaces, and one surface (KPK) obtained by empirical fitting to the measured total differential cross section. It is found that the total elastic, inelastic, and differential cross sections are very sensitive to the long-range attractive terms in the potential, and the differential cross sections are also found to be significantly dependent upon the topography of the repulsive regions of the surface. Consequently, differential cross sections are very sensitive probes of surface topography and should be the data of choice for purpose of empirical adjustment of a surface. In contrast, the relaxation rates of a depleted rotational level are found to be insensitive to the details of the surface. In addition, the relaxation rate and total inelastic cross section out of state j are found to be almost independent of the particular j state involved. Consideration of the microscopic details leading to these results suggests that similar behavior will be observed in other systems that are nearly classical with closely spaced energy levels. Of the surfaces investigated, the KPK surface gives results that are in closest agreement with experiment. The electron–gas and SCF surfaces, when augmented by a van der Waals attractive term, give similar results which are almost as good as those obtained on the empirically adjusted KPK surface. This suggests that a reasonable surface for a closed-shell system can be obtained by either procedure. The IOSA results for the relaxation rates and total inelastic cross sections are found to be in excellent agreement with quasiclassical trajectory calculations. However, the degree of agreement for quantities associated with state-to-state transitions is reduced.

I. INTRODUCTION

The theoretical investigation of collision dynamics in polyatomic systems is difficult. Generally, it is impossible to obtain accurate *ab initio* potential-energy surfaces or to carry out converged close-coupling calculations of the relevant cross sections. Consequently, one must employ potential-energy surfaces that may not be sufficiently accurate and use approximate methods for computing the scattering dynamics. For this reason, it is important to determine how well the available surface representations describe the system, and, if possible, to determine the exact nature of the major defects that may be present. It is likewise important to determine the extent to which the approximate scattering methods employed agree with one another and with the results of converged close-coupling studies, when they are available. As part of this evaluation, a comparison of computed results with those obtained from experimental measurement is generally made. When this procedure is employed, the question of the sensitivity of the data to the details of the potential-energy surface and to the computational procedure becomes crucial. In particular, it is necessary to determine what type of data is best suited to an evaluation of different features of the surface.

In our laboratory, we have been conducting theoretical studies of the inelastic collision dynamics in (CO_2, H_2), (CO_2, D_2),[1] and (CO_2, He)[2] systems. Rotational–translational energy transfer processes are of crucial importance[3–7] in the interpretation and description of laser processes, molecular-beam experiments, microwave broadening, spin–lattice relaxation of NMR signals, ultrasonic absorption and dispersion, thermal conductivity and transpiration, shock wave propagation, and intermolecular interactions. In addition, a comparison of experimental results with theoretical prediction provides a very useful test of the surfaces employed and of the approximate scattering methods used. Moreover, the use of CO_2 as a gain medium in lasers[7] that contain He as a diluent makes the (He, CO_2)[2,6–18] system a particularly attractive one to study.

At present, the available experimental data related to (He, CO_2) rotational energy transfer consists of relaxation rate measurements of CO_2 in the (00^01) vibrational level,[8,14,15] measurements of the total differential[9] and integral[16] cross sections for the system, and some data related to transport coefficients[17] and pressure broadening.[10(a)]

Several theoretical investigations of this system have been reported to date. Two of these are most pertinent to the present study.[2,11] Preston and Pack[11] have computed the rate of rotational relaxation of CO_2 (001) out of the $j=19$ rotational state using quasiclassical trajectory methods and an electron–gas potential-energy surface.[12] Their results demonstrated the importance of large Δj transitions in the relaxation process. The computed relaxation rate was in reasonable accord with the measured result[14,15] but was somewhat too large. It was therefore concluded that the relaxation calculation was very sensitive to small errors in the potential-energy surface and that such an error was giving a rotational

[a)]Supported in part by NSF Grant CHE 78-25563.
[b)]On leave from M. L. V. Govt. College Bhilwara, Rajasthan, India.

 0021-9606/81/172163-14$01.00

inelasticity that was too large. More recently, Stroud and Raff[2] have carried out quasiclassical trajectory calculations on the CO_2–He system using three different potential-energy surfaces: an *ab initio* SCF surface,[2] the electron–gas surface computed by Parker, Snow, and Pack,[12] and a surface obtained by Keil, Parker, and Kuppermann[9] by deconvolution of measured total differential cross sections. Thermally averaged, state-to-state integral, and differential inelastic cross sections were computed on each of these surfaces. It was found that at very low collision energies, the attractive forces play a major role in the collision dynamics, but at energies in excess of 0.01 eV, the importance of this feature decreases, and the inner repulsive region of the surface assumes the dominant role in determining the course of a collision. At such energies, it was found that the computed cross section from all surfaces were in reasonable agreement.

It is not clear how sensitive the relaxation measurements are to the details of the surface. Preston and Pack[11] concluded that such measurements were more sensitive than one would expect. However, the near agreement obtained by Stroud and Raff[2] between cross sections computed on three very different surfaces tends to suggest that such data might actually be rather insensitive to the topographical details of the surface. In any event, if the relaxation data is sensitive to the intermolecular potential, the most crucial topographical features are not known. Similar questions may be raised with regard to the integral and differential cross section measurements.

Preston and Pack[11] have shown that there is a significant decrease in the state-to-state integral cross section as Δj increases. The results obtained by Stroud and Raff[2] corroborate this point, and the result is consistent with the relaxation data reported by Jacobs, Thomas, and Pettipiece.[14(b)] Such a result would seem to suggest that one might observe a significant variation in the overall relaxation rate for different rotational states of CO_2. At present, the total relaxation rate of only one state $j=19$ has been measured, and no theoretical studies of the j dependence of this rate have been reported.

In the present paper we report the results of infinite-order sudden approximation calculations related to elastic and rotationally inelastic processes in the rigid rotor (CO_2, He) system. Six potential-energy surfaces have been utilized in the investigation, the three previously examined by Stroud and Raff[2] and three additional composite surfaces constructed so as to permit a more unequivocal assessment of the importance of different surface features to be made. Differential total cross sections, the complete state-to-state integral cross section matrix, and total elastic and inelastic cross sections as a function of energy have been computed. From the results, the rotational relaxation rate for rotational state $j(0 \le j \le 33)$ has been obtained as a function of temperature. Isotope effects for ^{3}He have been examined, and where possible, comparison is made with the trajectory results reported by Preston and Pack[11] and by Stroud and Raff.[2]

The potential-energy surfaces are described in Sec. II. Pertinent aspects of the theory are reviewed in Sec. III. Computational details and results are given in Sec. IV, and a summary is given in the final section.

II. POTENTIAL-ENERGY SURFACES

For the CO_2–He system, Parker, Snow, and Pack[12] have computed a potential-energy surface $V_{EG}(r,\gamma)$ using the electron–gas method:

$$V_{EG}(r,\gamma) = V_{HF}(r,\gamma) + V_{cor}(r,\gamma) , \tag{1}$$

with

$$V_{HF}(r,\gamma) = \sum_{k=0}^{4} v_{2k}^{HF}(r) P_{2k}(\cos\gamma) \tag{2}$$

and

$$V_{cor}(r,\gamma) = \sum_{k=0}^{4} v_{2k}^{cor}(r) P_{2k}(\cos\gamma) , \tag{3}$$

where

$$v_n^{HF}(r) = A_{n1} \exp(A_{n2} r + A_{n3} r^2) , \tag{4}$$

$$v_n^{cor}(r) = -B_{n1} \exp(B_{n2} r + B_{n3} r^2) . \tag{5}$$

The parameters A_{ni} and B_{ni} $(n=0, 2, 4, 6, 8;\ i=1, 2, 3)$ have been given in Table IX of Ref. 12.

Parker *et al.*[12] found that $V_{EG}(r,\gamma)$ obtained via Eqs. (1)–(5) lacks sufficient attractive interaction at large distances. To compensate for this deficiency, Eq. (5) was modified by incorporation of the van der Waals potential previously obtained by Pack.[13] The modified form of Eq. (5) is

$$v_n^{cor}(r) = \begin{cases} -B'_{n1} \exp(B'_{n2} r + B'_{n3} r^2) , & r \le r_n , \\ -C_6(n) r^{-6} - C_8(n) r^{-8} , & r \ge r_n . \end{cases} \tag{6}$$

The parameters B'_{n1}, $C_6(n)$, $C_8(n)$, and r_n have been given in Table XI of Ref. 12.

We have used the electron–gas potential defined by Eqs. (1)–(4) and (6). Hereafter, this potential is denoted by EG1. Contour maps of this surface are given in Refs. 2, 6, and 11. To investigate the effects of the long-range attractive terms, we have also utilized a potential defined by Eqs. (1) and (2) with $V_{cor}(r,\gamma)=0$. This potential is denoted by EG2. Finally, it is of some interest to examine the dynamics on a surface having a shallow attractive well which is computed by the electron–gas method alone, i.e., the potential defined by Eqs. (1)–(5). This surface is labeled EG3.

A splinefitted *ab initio* surface (SAI) for this system has previously been reported by Stroud and Raff.[2] The (SAI) surface does not contain the V_{cor} term due to lack of configuration mixing in the SCF wave function description of the system. To compensate, Eq. (6) using the same parameters as given in Table XI of Ref. 12 has been combined with the SAI surface. The surface so obtained is denoted SAI1. Like surface EG2, the SAI potential does not contain long-range attractive forces. We shall therefore denote it as SAI2, parallel to the notation employed for the electron–gas type surfaces.

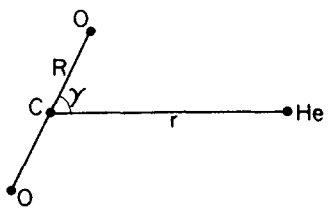

FIG. 1. Internal coordinates for the rigid rotor CO_2–He system.

The SAI and EG surfaces have been computed with the CO_2 atoms fixed in their equilibrium positions. Since the average length of the CO_2 molecule in the (001) vibrational state is less than 0.4% greater than that of the (000) state, we expect that these surfaces represent both states to a comparable degree of accuracy. The surfaces may, of course, be employed to investigate helium isotope effects in the system.

For comparison purposes, calculations have also been carried out for the (KPK) potential obtained by Keil, Parker, and Kuppermann[9] by deconvolution of their measured total differential cross sections. Contour maps for the (KPK) and (SAI2) surfaces have been given elsewhere.[2,9]

III. THEORY

A. Cross sections

The infinite-order sudden approximation (IOSA) has been described in detail by Parker and Pack.[6] For the convenience of the reader and to facilitate the description of the numerical procedures employed in the present work, we outline here the IOSA results pertinent to an atom–linear rigid rotor system.

The Schrödinger equation for the system (Fig. 1) is given by

$$(E-H)\psi=0\ , \tag{7}$$

where the Hamiltonian H can be written as

$$H=-\frac{\hbar^2}{2\mu r}\frac{\partial^2}{\partial r^2}r+\frac{L_{0\rho}^2}{2\mu r^2}+\frac{j_{0\rho}^2}{2I_0}+V(r,\gamma)\ . \tag{8}$$

Here μ is the atom–molecule reduced mass; I_0 is the moment of inertia of the molecule; $V(r,\gamma)$ is the interaction potential; $L_{0\rho}^2$ represents the operator corresponding to the square of the orbital angular momentum of the atom relative to the molecule; and $j_{0\rho}^2$ stands for the operator corresponding to the square of the molecular angular momentum.

The wave function ψ may be expanded as

$$\psi=\sum_{j''l''}|JMj''l''\rangle r^{-1}G_{j''l''}^{I}(r)\ , \tag{9}$$

where the $G(r)$ are radial channel wave functions and the superscript I denotes the set of initial quantum numbers J, M, j, and l. j'' and l'' refer to the usual quantum numbers corresponding to eigenvalues of operators $j_{0\rho}^2$ and $L_{0\rho}^2$, respectively. Similarly, J and M refer to the quantum numbers corresponding to the total angular momentum, i.e.,

$$|JMjl\rangle=\sum_{m_j}\sum_{m_l}C(jlJ;m_jm_lm)Y_{jm_j}(\hat{R})Y_{lm_l}(\hat{r})\ . \tag{10}$$

Here C represents the Clebsch–Gordan coefficients and other notations have their usual meaning.

Using Eqs. (7)–(10) and the orthonormal property of $|JMjl\rangle$, one can obtain the usual set of coupled radial equations:

$$\left[\frac{d^2}{dr^2}+k_{j'}^2-l'(l'+1)/r^2\right]G_{j'l'}^{I}(r)=\frac{2\mu}{\hbar^2}\sum_{j''l''}\langle JMj'l'|V|JMj''l''\rangle G_{j''l''}^{I}(r)\ , \tag{11}$$

with

$$k_{j'}^2=\frac{2\mu}{\hbar^2}\left[E-\frac{\hbar^2j'(j'+1)}{2I_0}\right]\ . \tag{12}$$

Equation (11) is difficult to solve, particularly when a large number of scattering channels must be included. The IOSA method[6] simplifies the problem by replacement of $L_{0\rho}^2$ and $j_{0\rho}^2$ by some suitable constants, such as their isolated eigenvalues. With this modification, Eq. (8) becomes

$$\left[-\frac{\hbar^2}{2\mu r}\frac{d^2}{dr^2}r+\frac{\bar{l}(\bar{l}+1)\hbar^2}{2\mu r^2}+\frac{\bar{j}(\bar{j}+1)\hbar^2}{2I_0}+V(r,\gamma)\right]\psi=E\psi\ , \tag{13}$$

where $\bar{l}$ and $\bar{j}$ are some appropriate values of l and j. Substituting

$$\psi=\frac{g^{\bar{j}\bar{l}}(r,\gamma)}{r} \tag{14}$$

in Eq. (13), one obtains

$$\left[\frac{d^2}{dr^2}+k_{\bar{j}}^2-\frac{\bar{l}(\bar{l}+1)}{r^2}\right]g^{\bar{j}\bar{l}}(r,\gamma)=\frac{2\mu}{\hbar^2}V(r,\gamma)g^{\bar{j}\bar{l}}(r,\gamma)\ . \tag{15}$$

Here

$$k_{\bar{j}}^2=\frac{2\mu}{\hbar^2}\left[E-\frac{\hbar^2\bar{j}(\bar{j}+1)}{2I_0}\right]\ . \tag{16}$$

Parker and Pack[6] now define

$$\tilde{G}_{j'l'}^{I}=i^{l-\bar{l}}\langle JMj'l'|g^{\bar{j}\bar{l}}(r,\gamma)|JMjl\rangle\ . \tag{17}$$

It can be shown with the help of Eqs. (15) and (17) and the completeness of the $|JMjl\rangle$ that

$$\left[\frac{d^2}{dr^2}+k_{\bar{j}}^2-\frac{\bar{l}(\bar{l}+1)}{r^2}\right]\tilde{G}_{j'l'}^{I}(r)=\frac{2\mu}{\hbar^2}\sum_{j''l''}\langle JMj'l'|V|JMj''l''\rangle\tilde{G}_{j''l''}^{I}(r)\ . \tag{18}$$

Comparing Eqs. (11) and (18), we note that as $[k_{j'}^2-l'(l'+1)/r^2]-[k_{\bar{j}}^2-\bar{l}(\bar{l}+1)/r^2]$, the exact radial function $G_{j'l'}^{I}(r)$ approaches the approximate radial function $\tilde{G}_{j'l'}^{I}(r)$.

In our computations, we have chosen $\bar{l}$=final orbital quantum number. For this choice the following results for the various cross sections may be obtained.[6]

1. *State-to-state cross sections*

We have

$$\sigma(j'\leftarrow j)=\frac{k_0^2}{k_j^2}\sum_{j''}C^2(jj''j';000)\sigma(j''\leftarrow 0)\ , \tag{19}$$

where

$$\sigma(j'' \leftarrow 0) = \frac{\pi}{(2j''+1)k_0^2} \sum_{l'} (2l'+1) |t_{j''}^{\bar{j}l'}|^2 , \tag{20}$$

with

$$t_{j''}^{\bar{j}l'} = (j''+\tfrac{1}{2}) \int_{-1}^{1} \{1 - \exp[2i\eta_{l'}^{\bar{j}}(\gamma)]\} P_{j''}(\cos\gamma) d\cos\gamma . \tag{21}$$

The phase shifts $\eta_{l'}^{\bar{j}}$ are determined[19,20] by solving Eq. (15).

Further, we choose $\bar{j}=j$, so that $k_{\bar{j}}$ corresponds to the initial energy

$$k_{\bar{j}} = k_j = k = \left(\frac{2\mu E_R}{\hbar^2}\right)^{1/2} . \tag{22}$$

Here E_R represents initial relative translation energy of the system.

2. *Differential and total cross sections*

Without distinguishing elastic or inelastic collisions, the expressions for the differential cross section $I(\theta)$ and total cross section σ_{Total} are

$$\sigma_{\text{Total}} = \frac{1}{2} \int_{-1}^{1} \sigma(\gamma) d\cos\gamma \tag{23}$$

and

$$I(\theta) = \frac{1}{2} \int_{-1}^{1} I(\gamma|\theta) d\cos\gamma , \tag{24}$$

where

$$\sigma(\gamma) = \frac{4\pi}{k^2} \sum_{l'} (2l'+1) \sin^2\eta_{l'}^{k}(\gamma) \tag{25}$$

and

$$I(\gamma|\theta) = |f^k(\gamma|\theta)|^2 , \tag{26}$$

with

$$f^k(\gamma|\theta) = \frac{i}{2k} \sum_{l'} (2l'+1) \times \{1 - \exp[2i\eta_{l'}(\gamma)]\} P_{l'}(\cos\theta) . \tag{27}$$

B. Relaxation rates

In some laser experiments[14,15] the population of the j (= 19) level of the (001) vibration state of CO_2 is quickly reduced to about half its original value and then monitored as it relaxes back into equilibrium with the other rotational levels of the same vibrational state. Preston and Pack[11] have discussed the kinetics for the relaxation of such a depleted level of CO_2 due to collisions with rare gas atoms. It has been shown[11] that for such a system the population density of the jth level n_j relaxes as follows:

$$\frac{dn_j(t)}{dt} = \left[\sum_{j' \neq j} k(j' \leftarrow j)\right] n_A [n_j(\infty) - n_j(t)] , \tag{28}$$

i.e., the relaxation time τ is given by

$$\tau^{-1} = k_{\text{out}}(j) n_A . \tag{29}$$

$k_{\text{out}}(j)$ is the rate coefficient for the relaxation. Preston and Pack[11] have shown that

$$k_{\text{out}}(j) = \sum_{j' \neq j} k(j' \leftarrow j) . \tag{30}$$

Here n_A represents the number of atoms of He per cm^3. The state-to-state thermal rate constant $k(j' \leftarrow j)$ is related to the state-to-state cross sections by

$$k(j' \leftarrow j) = k(j' \leftarrow j; T) = (8k_B T/\pi\mu)^{1/2} (k_B T)^{-2} \int_0^{\infty} \sigma(j' \leftarrow j; E_R) \times \exp(-E_R/k_B T) E_R \, dE_R . \tag{31}$$

Here k_B and T represent Boltzmann's constant and temperature, respectively.

IV. RESULTS

A. Computational procedures

Calculations have been performed over the energy range from 0.00002 to 1.0 eV. The number of phase shifts computed varies with energy. At 0.012 eV, 60 values were computed for each angle γ. This number increases to 300 for an energy of 1.0 eV. At energies of 0.012 eV or greater, the phase shifts have been computed using a 10-point Gauss–Mehler quadrature of the WKB phase shift equation.[19] Below 0.012 eV, quantum phase shifts have been computed using Johnson's procedure.[20]

Integration of Eqs. (21), (23), and (24) over γ have been performed by 96-point Gauss–Legendre quadrature. Eight-point Gauss–Laguerre quadrature has been used for evaluating the rate coefficients in Eq. (31).

In the computation of the relaxation rates at 450 K, the cross sections $\sigma(j' \leftarrow j)$ have been calculated at the eight points of Gauss–Laguerre quadrature. For other temperatures, the cross sections at other desired energy values have been obtained by cubic spline interpolation using as node values the 8 G points at 450 K and cross sections computed at 0.012 and 1.0 eV. When the temperature is 500 K or higher, cross sections at energy values in excess of 1.0 eV are required. In all cases, these cross sections were taken to be zero. Within the range of temperatures investigated in this study ($T \leq 900$ K), this approximation does not significantly decrease the accuracy of the calculations since the corresponding weight factors of Gauss–Laguerre quadrature are very small. For example, at 900 K, the weight factors corresponding to the first, second, sixth, seventh, and eighth points of Gauss–Laguerre quadrature which correspond to the energy values 0.031750, 0.10741, 0.93611, 1.3378, and 1.9068 eV are, respectively, 0.1876, 0.4390, 0.00031, 3.35×10^{-6}, and 4.72×10^{-9}.

B. Total cross sections

Total cross sections (elastic + inelastic) for CO_2–He and CO_2–^{3}He have been computed as a function of energy on each of the potential surfaces. The results are tabulated in Table I.

At higher energies, the repulsive part of the potential dominates the interaction. At lower energies, the long-range attractive terms make the major contribution to σ_{Total}. At all energies, the attractive and repulsive

TABLE I. Total (elastic+inelastic) cross sections in Å^2 as a function of relative translational energy for CO_2–He and CO_2–^{3}He.

	CO_2–He						CO_2–He^3
Energy (eV)	EG1	SAI1	KPK	EG2	SAI2	EG3	SAI1
0.012000	173.7	194.2	239.4	87.59	83.83	72.69	182.6
0.015875	164.4	180.1	217.2	86.79	82.66	72.61	170.7
0.053706	116.4	129.4	121.9	82.49	77.81	71.50	118.8
0.114638	90.98	99.50	88.09	79.29	74.71	70.09	90.85
0.200946	78.21	82.66	73.42	76.83	72.39	68.73	76.41
0.316495	71.07	72.81	67.22	74.78	70.48	67.48	68.29
0.468053	66.58	66.55	62.46	72.97	68.80	66.33	63.27
0.668911	63.49	62.30	59.94	71.33	67.29	65.21	59.18
0.953395	61.08	59.10	58.30	69.76	65.80	64.06	57.18
1.000000	60.76	58.73	58.03	69.50	65.61	63.92	56.87

forces tend to act in opposite directions, and there is a partial cancellation effect. Consequently, we note that although σ_{Total} (EG2) $>\sigma_{\text{Total}}$ (SAI2) at all energies, addition of the same attractive term [Eq. (6)] to both surfaces to produce EG1 and SAI1 reverses the inequality at low energies, i.e., σ_{Total}(SAI1) $>\sigma_{\text{Total}}$(EG1) at low energies. The more efficient repulsive forces on surface EG2 more effectively balance the effect of the attractive terms of Eq. (6) than is the case for the SAI2 surface. The inequality therefore reverses.

The competing effect of the attractive and repulsive forces upon σ_{Total} has also been demonstrated by computation of σ_{Total} at 0.012 eV on surface EG4 defined to be

$$V_{\text{EG4}} \equiv V_{\text{EG1}} - \tfrac{1}{2}V_{\text{HF}} = V_{\text{cor}} + \tfrac{1}{2}V_{\text{HF}} \ . \tag{32}$$

This reduction of the total repulsive term produces the expected increase in σ_{Total}(EG4) $= 187.5$ Å^2 $>\sigma_{\text{Total}}$(EG1).

We may also note from Table I that σ_{Total}(EG2) $>\sigma_{\text{Total}}$(EG1) at higher energies, i.e., the total cross section increases as the ratio of the magnitudes of the repulsive to attractive parts of the potential increases. This inference is in qualitative accord with similar conclusions recently reported by Eno and Rabitz.[21]

Butz, Feltgen, Pauly, and Vehmeyer[16] have measured the variation of an effective total cross section σ_{eff} with the velocity V_1 of a monochromatic He beam colliding with CO_2 at a fixed temperature. Parker and Pack[6] have previously reported a comparison of the IOSA results for the EG1 surface with their data. A comparison of the computed and measured slopes suggested that EG1 is somewhat too repulsive. Recently reported QCT calculations support this view.[2] The magnitude of σ_{eff} was also found to be too low at lower He beam velocities.

Figure 2 shows a similar comparison of σ_{eff} for each of the surfaces with the experimental data.[16] A 13-point Gauss–Hermite quadrature was used to average the cross sections over the Maxwell–Boltzmann distribution of CO_2 speeds. The SAI1 surface is seen to be in better accord with experiment, both with regard to magnitude and slope, than is the case for the EG1 surface. However, SAI1 is not sufficiently accurate to reproduce the finer details such as the curvature in the range $300 < V_1 < 1000$ m/s. In this range, the SAI1 result exhibits a positive curvature whereas the Butz *et al.*[16] results show a negative curvature. The results obtained on the KPK surface are rather remarkable. The magnitudes, slopes, and curvatures are predicted with almost quantitative accuracy over the entire velocity range.

There is a very little isotope effect for the ^{4}He–^{3}He systems. For each energy, the total cross sections decrease slightly for ^{3}He, which is qualitatively what one would expect from simple considerations of mass difference of the collision partners.

Although quasiclassical trajectory calculations (QCT) have been carried out on this system by Preston and Pack[11] and by Stroud and Raff,[2] no results for the total collision cross sections were reported. Stroud[22] has attempted such calculations and found that it is very difficult to obtain accurate results using the QCT method. The problem resides in accurately computing the contribution of trajectories scattered at angles near 0° to the elastic component of the total cross section. Such trajectories account for the major fraction of this cross section. Classically, these trajectories are associated

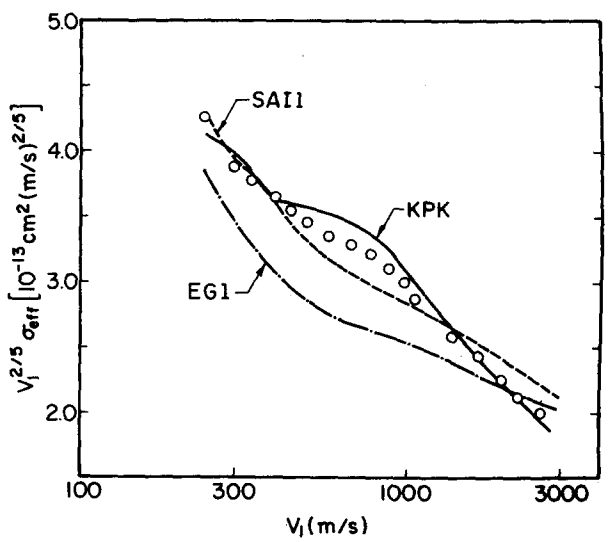

FIG. 2. Variation of velocity-averaged total integral cross sections with helium beam velocity V_1. (o o o o experiment—see Ref. 16. (-·-·) surface EG1. (- - -) surface SAI1. (—) surface KPK.

TABLE II. Total inelastic integral cross sections (in Å^2) out of the initial $j=19$ level as a function of the relative collision energy (in eV) for various potential-energy surfaces.

Energy (eV)	CO_2–He					CO_2–^{3}He
	EG1	SAI1	KPK	EG2	SAI2	SAI1
0.012000	45.9	46.0	40.3	32.3	29.3	44.7
0.015875	43.2	42.7	37.8	33.1	30.1	41.4
0.053706	38.2	35.6	31.2	34.7	32.3	34.5
0.114638	35.2	33.5	29.5	34.4	32.4	32.7
0.200946	34.1	32.4	28.9	33.9	32.1	31.6
0.316495	33.1	31.6	28.9	33.4	31.7	30.9
0.468053	31.9	30.6	28.3	33.1	31.1	30.1
0.668911	30.8	29.6	27.7	31.4	30.2	29.1
0.953395	29.6	28.5	27.0	30.3	29.2	28.1
1.00000	29.5	28.4	27.0	30.1	29.0	27.9

with large impact parameter collisions. Consequently, to obtain an accurate statistical measure of their contribution, it is necessary to utilize a very large maximum impact parameter and to compute a prohibitively large number of trajectories. If this is not done, Stroud's results show that the statistical error in σ_{Total} will approach a factor of 2. In essence, a QCT calculation is not a feasible procedure for the computation of total elastic cross sections.

C. Total inelastic cross sections

The total inelastic cross sections σ_{inel} for the initial state $j=19$ are tabulated in Table II as a function of energy for each of the potential-energy surfaces. The results for the CO_2–^{3}He system on the SAI1 surface have also been given in the table. Table III gives the total inelastic cross sections for the SAI1 surface for initial j states (1, 5, 9, 13, 17, 19, 21, 25, 29, and 33) as a function of energy.

For the potential-energy surfaces that include a long-range attractive term, the total inelastic cross section exhibits a monotonic decrease with increasing energy. For the surfaces missing this term, the energy dependence of σ_{inel} is very weak, and a maximum in the σ_{inel} vs energy curve is obtained.

At higher energies (~1.0 eV), the differences in the values for σ_{inel} between the SAI1 and SAI2 surfaces or between EG1 and EG2 is less than 3%. Clearly, in this energy range, the long-range attractive term is of negligible importance. Suzukawa, Wolfsberg, and Thompson[23] have previously reported similar results for QCT calculations of inelastic energy transfer in CO_2–noble gas systems.

An interesting feature of the total inelastic cross section is shown in Table III. At a given energy, σ_{inel} is almost independent of the initial rotational state of the CO_2 molecule. Since the state-to-state cross sections are strongly dependent upon the energy spacing between initial and final states, and since this spacing is linearly dependent upon j, the near independence of σ_{inel} upon j is somewhat surprising. In general, this behavior is a result of the fact that transitions associated with large Δj have appreciable cross sections in this system. Thus, σ_{inel} includes significant contributions from many state-to-state processes. The summation over all such transitions tends to average out the dependence of σ_{inel} upon j. Although Table III gives only the results on the SAI1 surface, qualitatively similar behavior is seen on each of the other surfaces.

The total elastic cross section σ_{el} may be obtained from a simple difference between the results given in Tables I and II. For the SAI1 and EG1 surfaces the ratio $(\sigma_{el}/\sigma_{inel})$ decreases with increasing energy. At low energy (~0.012 eV) its value is about 3. As the energy increases, this ratio is computed to approach 1.

^{3}He inelastic isotope effects are very similar to those obtained from the total cross sections. In general, they reflect the decreased efficiency of energy transfer as the mass difference between the collision partners increases.

A comparison of IOSA and QCT results for the total inelastic cross section is given in Fig. 3 and in Table IV. In Fig. 3, σ_{inel} for an initial rotational state $j=19$ on the EG1 surface has been plotted as a function of energy. The points are the QCT results obtained by Preston and Pack.[11] Table IV compares the present IOSA results with the QCT calculations reported by Stroud and Raff[2] on the SAI2, EG1, and KPK surfaces. In general, there is good to excellent agreement between the two

TABLE III. Total inelastic integral cross section (in Å^2) out of the initial j level as a function of the relative collision energy for the SAI1 surface.

j \ Energy (eV)	0.012000	0.015875	0.053706	0.114638	0.200946	0.316495	0.468053	0.668911	0.953395	1.000000
1	48.3	44.8	37.0	34.7	33.4	32.5	31.8	30.8	29.5	29.4
5	45.2	42.1	35.5	33.7	32.7	31.9	31.2	30.2	29.1	28.9
9	45.5	42.2	35.2	33.5	32.5	31.8	31.0	30.0	28.9	28.8
13	45.9	42.6	35.4	33.4	32.4	31.7	30.9	29.9	28.8	28.6
17	46.0	42.7	35.6	33.5	32.4	31.7	30.7	29.7	28.6	28.5
19	46.0	42.7	35.6	33.5	32.4	31.6	30.6	29.6	28.5	28.4
21	46.0	42.7	35.6	33.6	32.5	31.6	30.5	29.5	28.4	28.3
25	46.0	42.7	35.6	33.6	32.6	31.4	30.3	29.3	28.2	28.1
29	46.1	42.8	35.6	33.7	32.5	31.3	30.0	29.0	27.9	27.8
33	46.1	42.8	35.7	33.8	32.3	31.0	29.7	28.6	27.6	27.5

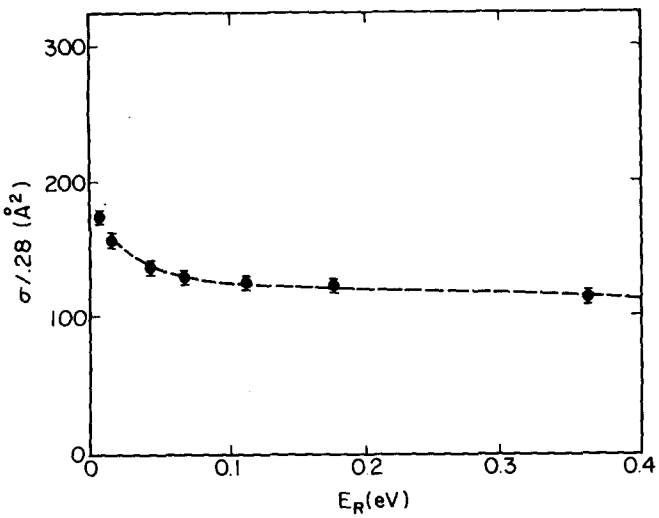

FIG. 3. Comparison of QCT (Ref. 11) and IOSA computations of the total inelastic cross section out of the $j=19$ state as a function of energy on the EG1 surface. (Points are the QCT results.)

methods even in the low-energy region where one might expect the accuracy of the IOSA model to be significantly reduced.

D. State-to-state integral cross sections

State-to-state integral cross sections $\sigma(j' \leftarrow j)$ for $(1 \leq j' \leq 65)$ with various initial j states have been evaluated at 10 different energies in the range 0.012 to 1.0 eV on each potential-energy surface. Typical results showing the dependence of $\sigma(j' \leftarrow j)$ upon initial and final states, relative translational energy E_R, and potential surface are given in Figs. 4–8. Comparison of IOSA and QCT results on the EG1, SAI2, and KPK surfaces are given in Tables V–VII.

Figures 4(a)–4(d) illustrate the variation of $\sigma(j' \leftarrow 19)$ with j' and E_R. The dependence of the state-to-state cross sections upon the initial rotation state is shown in Figs. 5(a) and 5(b). A comparison of the results for the SAI1 and SAI2 surfaces shows that at lower energies neglect of the long-range attractive term increases the cross sections for small Δj transitions and decreases those associated with large Δj. Consequently, the importance of multiple quantum transitions should increase in systems with larger van der Waals attractive interactions.

TABLE IV. Total inelastic cross sections at $E_R = 0.0616$ eV (in Å²).

	Initial $j=0$		Initial $j=16$	
	IOSA	QCT[a]	IOSA	QCT[a]
A. SAI2 surface				
Excitation	36.7	37.69	19.2	16.45
De-excitation	•••	•••	13.1	16.20
Total	36.7	37.69	32.3	32.65
B. EG1 surface				
Excitation	40.8	42.36	22.9	19.43
De-excitation	•••	•••	13.7	17.92
Total	40.8	42.36	36.6	37.35
C. KPK surface				
Excitation	34.6	34.42	19.0	16.15
De-excitation	•••	•••	11.1	15.04
Total	34.6	34.42	30.1	31.19

[a]Reference 2.

TABLE V. Comparison of quasiclassical trajectory (QCT) and IOSA state-to-state integral cross sections at a total relative energy of 0.0616 eV on the SAI2 surface for initial CO_2 j states of 0 and 16. Statistical uncertainties are shown in parentheses.

	$\sigma(j' \leftarrow 0)$ (Å²)		$\sigma(j' \leftarrow 16)$ (Å²)	
j'	IOSA	QCT[a]	IOSA	QCT[a]
0	•••	•••	0.0692	0.0989(0.046)
2	8.37	8.995(0.560)	0.334	0.3520(0.086)
4	5.66	6.022(0.441)	0.576	0.5731(0.122)
6	4.62	5.403(0.397)	0.869	1.167(0.175)
8	4.18	4.752(0.359)	1.30	1.589(0.221)
10	3.46	4.040(0.311)	1.87	2.615(0.294)
12	3.03	3.117(0.249)	2.85	3.622(0.359)
14	2.88	2.724(0.224)	5.24	6.187(0.487)
16	2.28	2.053(0.177)	•••	•••
18	1.35	0.697(0.099)	5.89	6.856(0.502)
20	0.598	0	3.59	3.985(0.366)
22	0.200	0	2.65	2.535(0.269)
24	0.0526	0	2.08	1.597(0.207)
26	0.0116	0	1.60	0.843(0.124)
28	0.00293	0	1.25	0.568(0.101)
30	0.00029	0	0.967	0.066(0.039)
32	0.00008	0	0.640	0
34	0.00004	0	0.334	0
36	0.00004	0	0.135	0

[a]Reference 2.

TABLE VI. Comparison of quasiclassical trajectory (QCT) and IOSA results for state-to-state integral cross sections at a total relative energy of 0.0616 eV on the EG1 surface for initial CO_2 j states of 0 and 16. Statistical uncertainties are shown in the parentheses.

	$\sigma(j' \leftarrow 0)$ (Å²)		$\sigma(j' \leftarrow 16)$ (Å²)	
j'	IOSA	QCT	IOSA	QCT[a]
0	•••	•••	0.0729	0.022(0.021)
2	7.10	7.890(0.599)	0.380	0.646(0.151)
4	5.17	6.405(0.515)	0.715	1.505(0.225)
6	4.39	4.897(0.433)	1.08	1.498(0.226)
8	3.90	4.609(0.420)	1.52	1.821(0.242)
10	3.31	4.103(0.380)	2.08	2.277(0.295)
12	3.08	3.542(0.342)	2.96	4.080(0.399)
14	2.80	2.821(0.286)	4.94	6.076(0.505)
16	2.41	2.561(0.265)	•••	•••
18	2.20	2.152(0.223)	5.51	6.118(0.495)
20	2.09	1.993(0.211)	3.64	4.794(0.426)
22	1.79	1.133(0.151)	2.82	2.644(0.299)
24	1.27	0.253(0.074)	2.29	2.143(0.253)
26	0.746	0	1.87	1.666(0.209)
28	0.374	0	1.58	0.998(0.163)
30	0.169	0	1.32	0.686(0.122)
32	0.0720	0	1.08	0.347(0.091)
34	0.0308	0	0.891	0.032(0.032)
36	0.0136	0	0.723	0

[a]Reference 2.

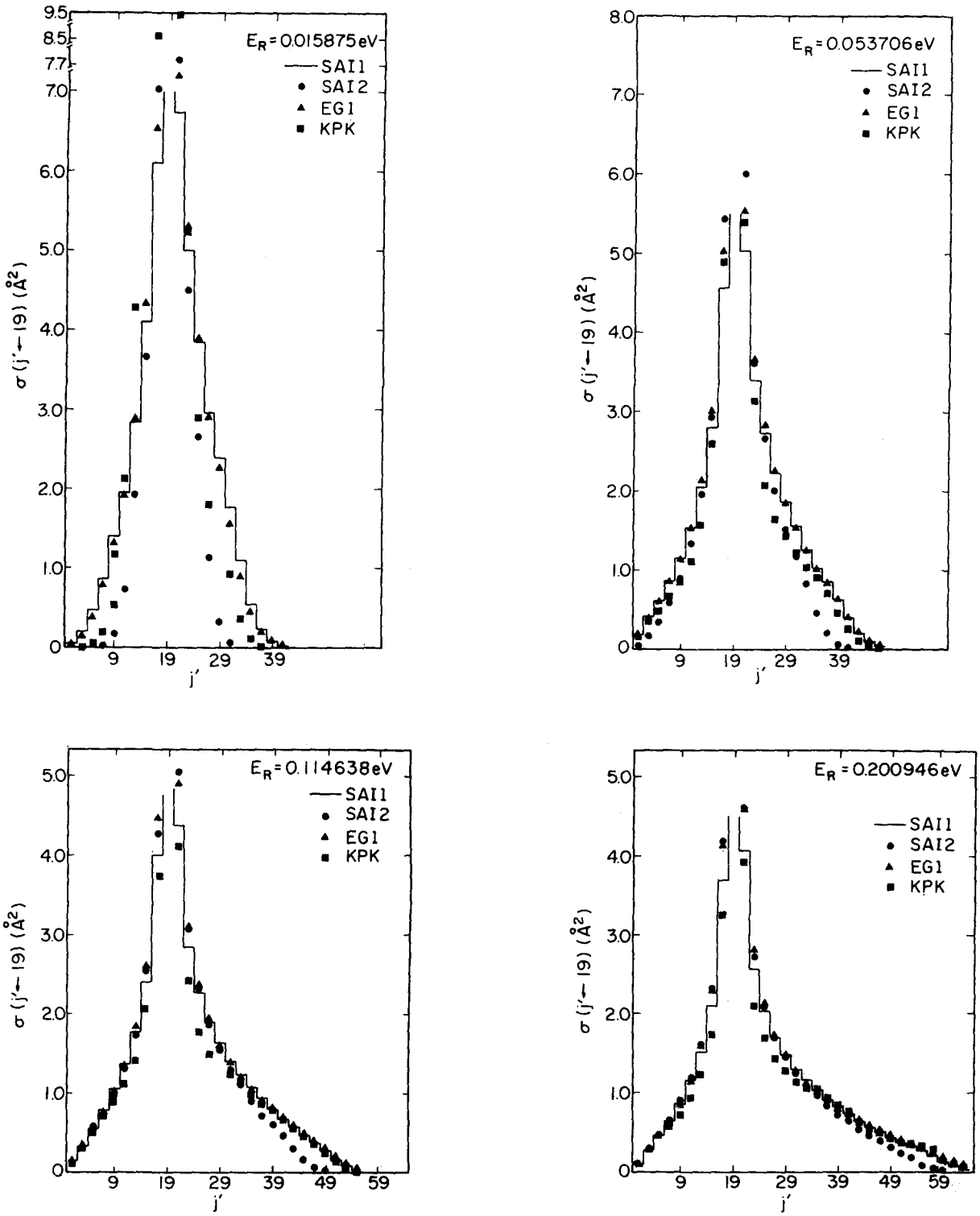

FIG. 4. Dependence of $\sigma(j' \rightarrow 19)$ upon j' for the SAI 1, SAI 2, EG 1, and KPK surfaces. (a) $E_R = 0.015875$ eV; (b) $E_R = 0.053706$ eV; (c) $E_R = 0.114638$ eV; (d) $E_R = 0.200946$ eV.

Except for small Δj transitions, surfaces EG1 and SAI1 yield nearly identical results for $\sigma(j' \leftarrow j)$ at all energies. Even for small Δj, the maximum differences are less than 12%. It would appear that SCF and electron–gas type calculations of the Hartree–Fock portion of the potential are essentially equivalent for closed-shell systems. If these representations are augmented by identical correlation terms, the resulting surfaces appear to be of comparable accuracy.

The KPK potential with its intermediate range Morse-type description is clearly very different from both EG- and SAI-type surfaces. This is illustrated most dramatically in Fig. 6, where the energy dependence of

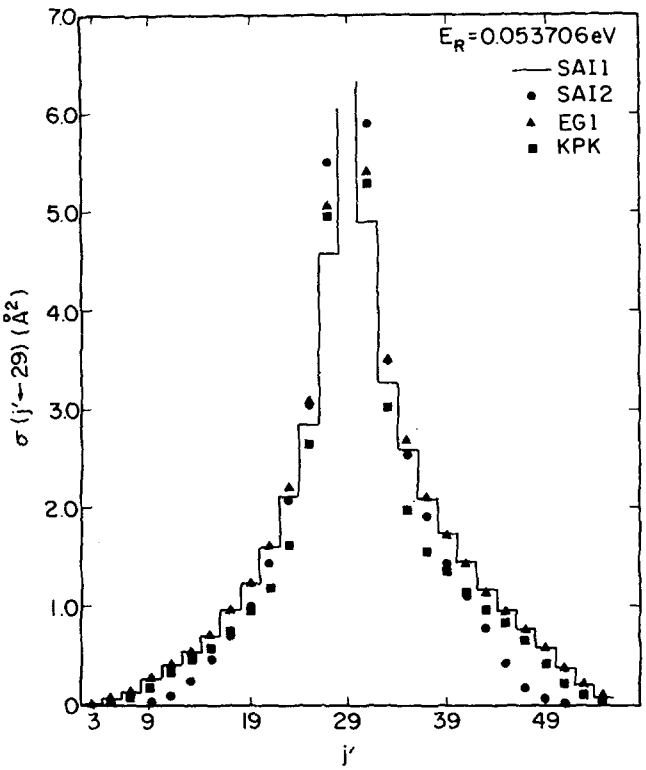

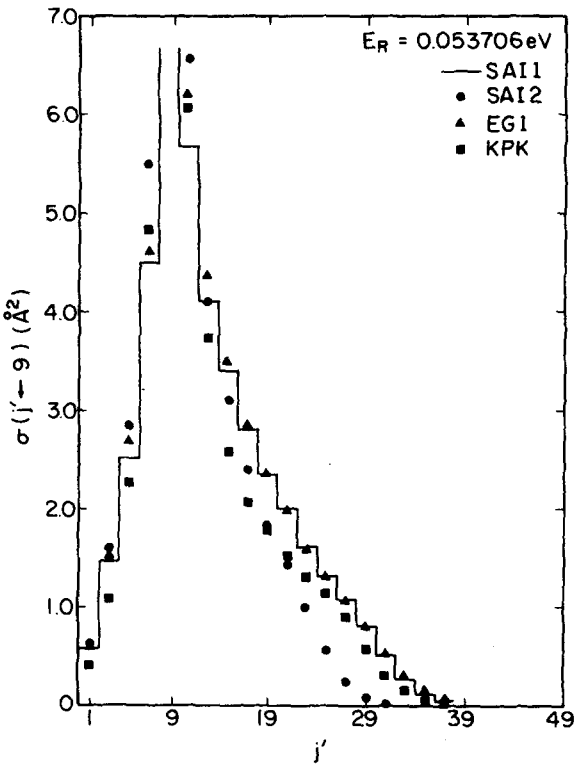

FIG. 5. Dependence of $\sigma(j' \leftarrow j)$ upon j' and j for the SAI 1, SAI 2, EG 1, and KPK surfaces at $E_R = 0.053706$ eV. (a) $j = 29$; (b) $j = 9$.

$\sigma(17 \leftarrow 19)$ is shown for each surface. The EG1, EG2, SAI1, and SAI2 results are roughly parallel curves, but the KPK surface predicts a much more rapid increase in $\sigma(17 \leftarrow 19)$ as E_R decreases.

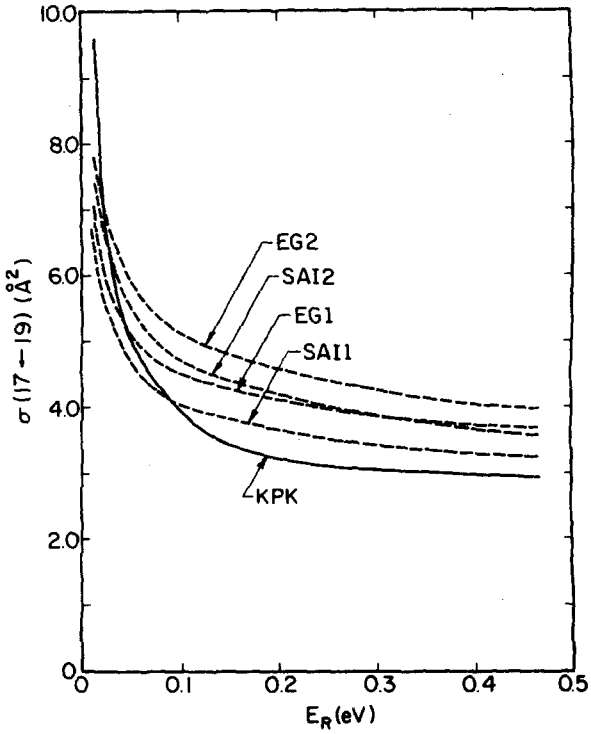

FIG. 6. Variation of $\sigma(17 \leftarrow 19)$ with energy on the EG 1, EG 2, SAI 1, SAI 2, and KPK surfaces.

The QCT results of Preston and Pack[11] and those of Stroud and Raff[2] are compared with the IOSA results in Figs. 7 and 8 and Tables V–VII. In general, relative to the IOSA results, QCT calculations tend to overestimate the cross sections for small Δj transitions and underestimate those for larger Δj. However, for processes associated with large Δj, the IOSA method becomes increasingly inexact, and the QCT results are more likely to be correct. The reverse is probably true for small Δj transitions.

For a given state-to-state transition, the QCT and IOSA results are in good accord at energies above 0.10 eV. Below this, the QCT results exceed those predicted

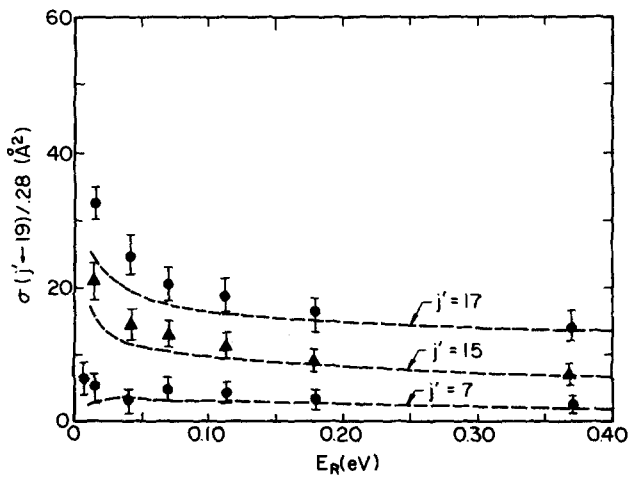

FIG. 7. Comparison of QCT (Ref. 11) and IOSA results for $\sigma(j' \leftarrow 19)$ as a function of energy on the EG 1 surface for $j' < 19$. (Points are the QCT results.)

TABLE VII. Comparison of quasiclassical trajectory (QCT) and IOSA results for state-to-state integral cross sections at a total relative energy of 0.0616 eV on the KPK surface for initial CO_2 j states of 0 and 16. Statistical uncertainties are shown in the parentheses.

	$\sigma(j' \leftarrow 0)$ (Å^2)		$\sigma(j' \leftarrow 16)$ (Å^2)	
j'	IOSA	QCT[a]	IOSA	QCT[a]
0	...	...	0.0706	0.155(0.055)
2	7.73	9.764(0.580)	0.351	0.488(0.093)
4	4.82	5.471(0.415)	0.626	0.974(0.141)
6	3.12	2.564(0.281)	0.875	1.018(0.147)
8	2.57	2.886(0.289)	1.14	1.403(0.179)
10	2.41	2.72(0.266)	1.54	1.592(0.190)
12	2.33	2.641(0.249)	2.43	2.830(0.267)
14	2.21	2.467(0.233)	4.69	6.580(0.434)
16	2.33	2.452(0.220)	...	...
18	2.39	2.344(0.197)	5.25	6.887(0.439)
20	2.04	1.043(0.119)	3.02	2.981(0.267)
22	1.33	0.068(0.027)	2.09	2.009(0.205)
24	0.750	0	1.70	1.388(0.166)
26	0.329	0	1.47	1.077(0.138)
28	0.136	0	1.29	1.011(0.126)
30	0.0655	0	1.12	0.678(0.099)
32	0.0230	0	0.986	0.120(0.037)
34	0.00687	0	0.821	0
36	0.00457	0	0.591	0

[a]Reference 2.

by IOSA calculations. It is not clear whether this difference at low energies is due to a breakdown of the classical model, the sudden approximation, or both.

The ^{3}He–^{4}He isotope effect is given in Table VIII for the $\sigma(j' \leftarrow 19)$ transition ($1 \leq j' \leq 49$) on the SAI1 surface. It is interesting to note that for excitations associated with small Δj and for some de-excitation processes, the ^{3}He cross sections frequently exceed those computed for ^{4}He. Nearly identical results are obtained for the KPK surface. Consequently, it would appear that such isotope effects are very insensitive to the details of the potential surface topography.

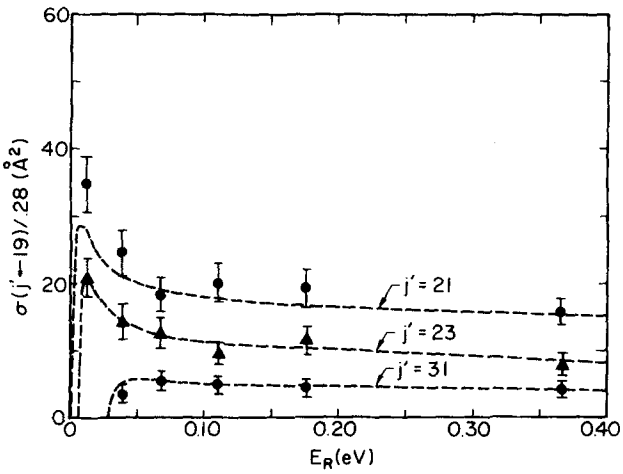

FIG. 8. Comparison of QCT (Ref. 11) and IOSA results for $\sigma(j' \leftarrow 19)$ as a function of energy on the EG1 surface for $j' > 19$. (Points are the QCT results.)

E. Relaxation of a depleted level

Using intense, short-pulsed CO_2 lasers, Abrams and Cheo[15] and Jacobs, Pettipiece, and Thomas[14(a)] have measured the rate of relaxation of the $CO_2(001, j = 19)$ rotational level at 450 K in mixtures of (CO_2–N_2) and (CO_2–He). Preston and Pack[11] have computed k_{out} (19) as a function of temperature for (CO_2–He) using QCT methods on surface EG1. They obtained a computed rate coefficient of $(6.1 \pm 0.2) \times 10^{-10}$ cm^3/s at 450 K. This result was about 85% larger than the experimentally reported value of $(3.3 \pm 0.5) \times 10^{-10}$ cm^3/s. It was concluded that the calculations were sensitive to small errors in the potential-energy surface and that such errors were primarily responsible for the major portion of the disagreement between the two results. However, our present calculations indicate that the relaxation rate is rather insensitive to the topography of the potential-energy surface.

We have computed the relaxation rate k_{out} (j) on each potential-energy surface as a function of temperature and j state. The temperature dependence of k_{out} (j) is

TABLE VIII. Comparison of state-to-state integral cross sections $\sigma(j' \leftarrow 19)$ in Å^2 for CO_2–He and CO_2–^{3}He (SAI1 surface).

	0.015875 eV		0.114638 eV		0.200946 eV		0.316495 eV	
j	CO_2–He	CO_2–^{3}He	CO_2–He	CO_2–^{3}He	CO_2–He	CO_2–^{3}He	CO_2–He	CO_2–^{3}He
1	0.055	0.019	0.15	0.14	0.12	0.13	0.10	0.11
5	0.47	0.26	0.55	0.57	0.46	0.48	0.39	0.41
9	1.39	1.26	1.05	1.05	0.88	0.91	0.75	0.91
13	2.84	2.80	1.77	1.77	1.52	1.60	1.52	1.39
17	6.09	6.49	4.00	4.12	3.69	3.81	3.69	3.53
21	6.73	7.17	4.39	4.53	4.07	4.16	4.07	3.91
25	3.85	3.80	2.26	2.32	2.04	2.06	1.84	1.91
29	2.38	2.18	1.63	1.63	1.48	1.48	1.39	1.38
33	1.09	0.61	1.24	1.18	1.16	1.13	1.12	1.08
37	0.23	0.08	0.93	0.84	0.92	0.88	0.91	0.86
41	0.029	0.0076	0.67	0.57	0.74	0.67	0.75	0.69
45	0.003	0.0006	0.47	0.30	0.58	0.49	0.62	0.56
49			0.26	0.079	0.44	0.35	0.51	0.44

given for each surface in Table IX, and the variation with j state is shown in Table X. Table XI illustrates the combined dependence upon both temperature and j state for the SAI1 surface.

The relaxation rate is always maximum for the EG1 surface. The results on SAI1 are intermediate between those for the EG1 and KPK surfaces. The differences, however, are small. The variation of $k_{out}(j)$ between surfaces EG1 and SAI1 is on the order of 5%. The KPK results are lower than those for SAI1 by only about 15%. Thus, in spite of rather significant variations in the topography of the attractive well and inner repulsive wall regions of these surfaces, there is little variation in the computed relaxation time.

The insensitivity for $k_{out}(j)$ to surface topography is also shown by the results on surfaces EG2, SAI2, and EG3. In each case, removal of the long-range attractive term decreases the computed relaxation rate, but the decrease is only 5%–14% on the SAI surfaces and 3%–11% on the EG surfaces with the larger decrease occurring at the lower temperatures. None of these variations are sufficiently large to account for the difference between the computed and measured values for k_{out} (19) at 450 K.

The present IOSA calculations predict that the rotational relaxation rate coefficient for the equilibration of a depleted j level will be nearly independent of j. This is shown clearly in Tables X and XI. This result is similar to the j independence of $\sum_{j'} \sigma(j' \leftarrow j)$ given in Table III.

Although we find $k_{out}(j)$ to be an insensitive function of j, the individual state-to-state transition rate coefficients $k(j' \leftarrow j)$ are strongly dependent upon Δj. For any given j state, $k(j' \leftarrow j)$ decreases as Δj increases. This result has been found experimentally by Jacobs *et al.*[14(b)] and has previously been obtained for the $j=19$ state by Preston and Pack.[11]

The QCT and IOSA results for $j=19$ at $T=450$ K are compared in Fig. 9. The agreement between the two is only fair. Relative to the IOSA calculations, the trajectory results[11] enhance the rates for large negative Δj transitions and underestimate those associated with large positive Δj transitions. However, the overall sum of the $k(j' \leftarrow j)$ over j' obtained by the two methods is in excellent agreement since the variations for negative Δj are nearly canceled by those for positive Δj. Consequently, computed relaxation rates are in good accord.

TABLE IX. Rotational relaxation rate constants $k_{out}(19)$ for the refilling of $CO_2(001; j=19)$ by collisions with $He/^3He$.

Temp. (K)	$k_{out}(19)\times 10^{10}$ (cm^3/s) CO_2–He EG1	SAI1	KPK	EG2	SAI2	EG3	CO_2–^{3}He SAI1
350	5.42	5.23	4.61	4.86	4.51	4.52	5.79
400	5.74	5.53	4.87	5.20	4.83	4.84	6.12
450	6.03	5.81	5.11	5.51	5.14	5.14	6.44
500	6.31	6.07	5.34	5.81	5.42	5.42	6.73
550	6.57	6.31	5.56	6.09	5.69	5.68	7.00
600	6.81	6.54	5.76	6.36	5.95	5.94	7.25
650	7.04	6.76	5.96	6.62	6.20	6.18	7.49
700	7.26	6.96	6.14	6.87	6.44	6.42	7.72
800	7.65	7.32	6.49	7.34	6.89	6.86	8.13
900	8.01	7.65	6.80	7.78	7.31	7.27	8.49

TABLE X. Rotational relaxation rate constants $k_{out}(j)$ for the refilling of $CO_2(001; j)$ by collisions with $He/^3He$ at 450 °K.

j	$k_{out}(j)\times 10^{10}$ (cm^3/s) CO_2–He EG1	SAI1	KPK	EG2	SAI2	EG3	CO_2–^{3}He SAI1
1	...	6.05	...	...	...	...	6.69
5	...	5.80	...	...	...	...	6.39
9	5.99	5.77	5.08	5.47	5.10	5.10	6.38
13	6.01	5.78	5.10	5.49	5.12	5.12	6.41
15	6.02	...	5.10	5.50	5.13	5.13	...
17	6.03	5.80	5.11	5.51	5.13	5.13	6.43
19	6.03	5.81	5.11	5.51	5.14	5.14	6.44
21	6.04	5.81	5.12	5.52	5.14	5.14	6.44
23	6.04	...	5.12	5.52	5.14	5.14	...
25	6.04	5.82	5.12	5.52	5.14	5.14	6.44
29	6.05	5.82	5.12	5.52	5.14	5.14	6.45
33	6.05	5.83	5.12	5.52	5.14	5.14	6.45

The lack of sensitivity of the relaxation rate to the potential-energy surface makes it unlikely that such measurements will enable the topographical details of the surface to be accurately determined. Furthermore, the independence of $k_{out}(j)$ to j suggests that this will be true even if the relaxation rates for a wide range of j states were to be measured.

The temperature dependence of $k_{out}(j)$ is very similar to that reported by Preston and Pack[11] for $j=19$. The increase of the relaxation rate coefficient with increas-

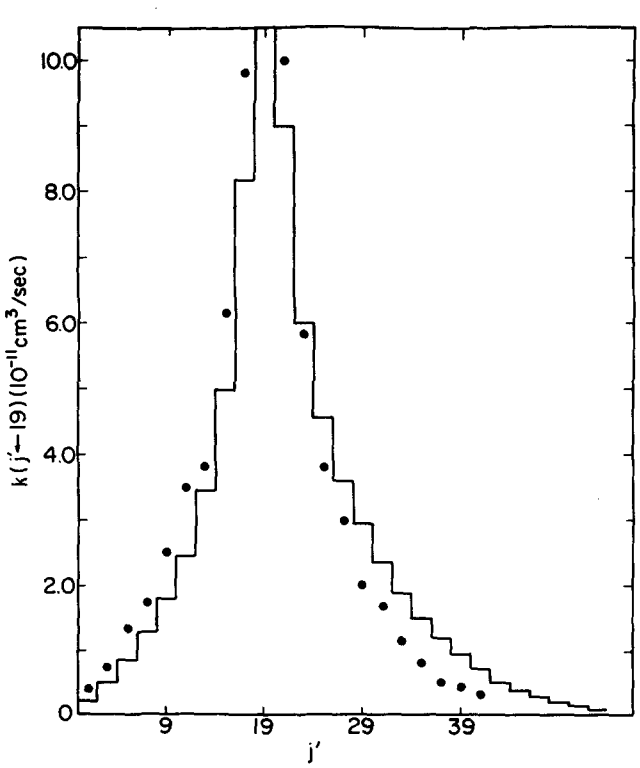

FIG. 9. Variation of state-to-state rate coefficients $k(j' \leftarrow 19)$ as a function of j' at 450 K on the EG1 surface. The histogram gives the IOSA results, and the points are QCT calculations taken from Ref. 11.

TABLE XI. Rotational relaxation rate constants $k_{out}(j)$ for the refilling of $CO_2(001; j)$ by collisions with He as a function of j and temperature for the SAI 1 surface.

j \ Temp. (K)	$k_{out}(j)\times 10^{10}$ (cm^3/s)									
	350	400	450	500	550	600	650	700	800	900
1	5.44	5.75	6.04	6.30	6.55	6.79	7.00	7.21	7.58	7.91
5	5.21	5.51	5.80	6.07	6.31	6.55	6.77	6.97	7.35	7.68
9	5.19	5.48	5.77	6.03	6.28	6.51	6.72	6.93	7.30	7.63
13	5.21	5.50	5.78	6.05	6.29	6.52	6.73	6.93	7.30	7.63
17	5.23	5.52	5.80	6.06	6.31	6.54	6.75	6.95	7.32	7.64
19	5.23	5.53	5.81	6.07	6.31	6.54	6.76	6.96	7.32	7.65
21	5.23	5.53	5.81	6.08	6.32	6.55	6.76	6.96	7.33	7.65
25	5.24	5.54	5.82	6.08	6.33	6.56	6.77	6.97	7.34	7.66
29	5.24	5.54	5.82	6.09	6.33	6.56	6.77	6.97	7.33	7.66
33	5.25	5.54	5.83	6.09	6.33	6.56	6.77	6.97	7.33	7.64

ing temperature is essentially a result of an increased collision frequency. This may be seen by noting that $[T^{-1/2}k_{out}(j)]$ is very nearly independent of temperature in the range $300 \leq T \leq 900$ K.

The ^{3}He–^{4}He isotope effect is given in Tables IX and X. The computed ^{3}He relaxation rate coefficient exceeds that for ^{4}He by about 10%. This is due to the increased collision frequency of the ^{3}He–CO_2 system which is proportional to $\mu^{-1/2}$. This should lead to a 14% difference in the two rates. The computed ratio is somewhat less since the ^{3}He–CO_2 collisions are less effective than those for the ^{4}He–CO_2 system.

F. Differential cross sections

Differential cross sections at a relative energy of 0.064 eV have been computed in the center-of-mass frame. Figure 10 gives the results for the SAI1 and KPK surfaces. It also shows the results for the CO_2–^{3}He system on the SAI1 surface. Figure 11 compares the differential cross sections obtained for the EG1 and EG2 surfaces.

Comparison of the results for the EG1 and EG2 surfaces shows that the differential cross sections are very sensitive to the long-range attractive terms in the potential. In the absence of such terms, the computed amplitudes of the resonance peaks are significantly reduced, and the positions of the maxima are shifted by 0.5°

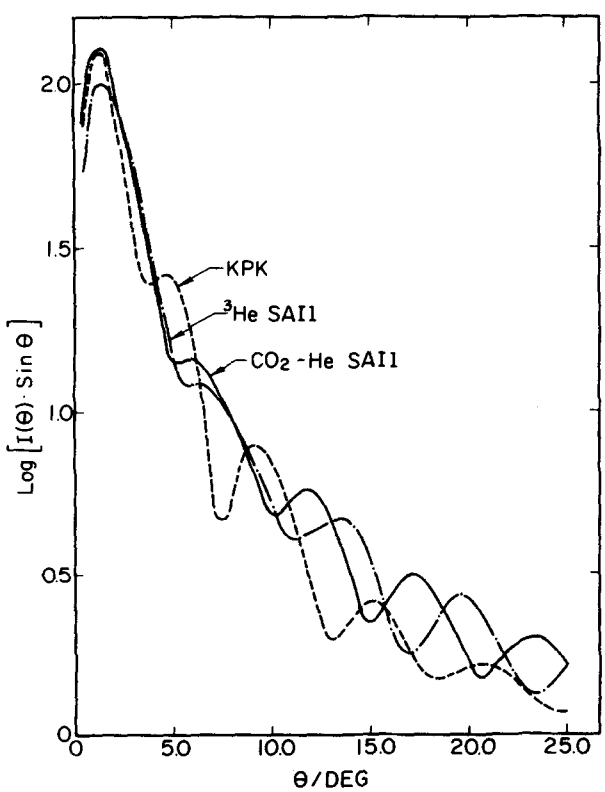

FIG. 10. Computed total differential cross sections at E_R = 0.064 eV for CO_2–^{4}He on the SAI 1 and KPK surfaces and for CO_2–^{3}He on the SAI 1 surface.

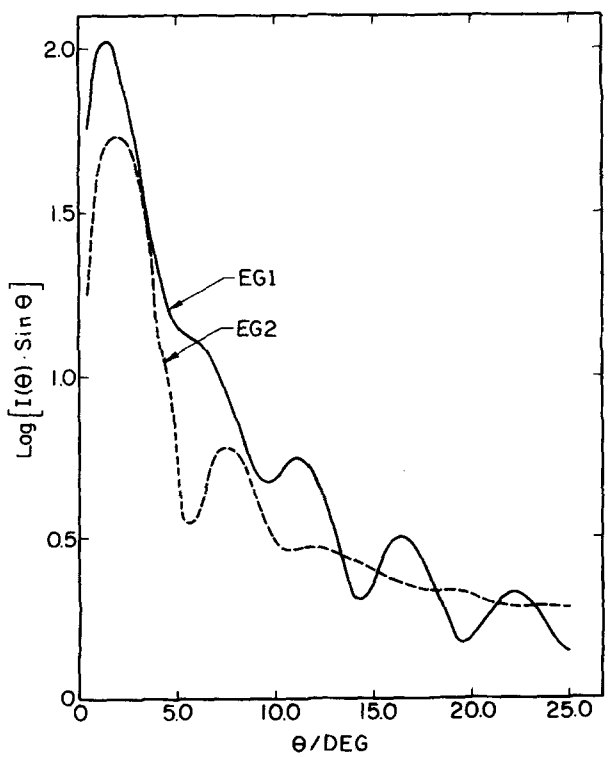

FIG. 11. Comparison of total differential cross sections at E_R = 0.064 eV on the EG1 and EG2 surfaces.

or more. The results obtained for the SAI2 surface relative to those for SAI1 show very similar effects.

Keil, Parker, and Kuppermann[9] have previously reported measurements of the (CO_2–He) total differential cross section and have adjusted the KPK potential so as to reproduce their laboratory data. Parker and Pack[6] have computed the total differential cross section on surface EG1 and found that while the shape and degree of damping are in reasonably good accord with experiment,[9] the calculated oscillations are out of phase by a constant amount. The results for the SAI1 surface given in Fig. 10 show that these oscillations are also out of phase with the KPK results by an essentially constant amount of 2.5°.

These results support the conclusions drawn by Pack[18] that the sensitivity of the total differential cross section to the potential-energy surface in systems of this type is sufficient to permit a reasonably accurate determination of the topography of both the long-range attractive and intermediate repulsive regions to be obtained by iterative fitting of the surface to such data. The results reported by Parker and Pack[6] and those of Fig. 10 suggest that the phase shift is sensitive to the intermediate range forces, and Fig. 11 clearly demonstrates the sensitivity of the amplitude to the long-range attractive potential. Furthermore, it appears that the same changes in potential required to bring the computed differential cross sections into accord with experiment also serve to improve the agreement of other computed properties. In the present case, this is seen to be true for both the total integral cross sections and the relaxation rate of a depleted level. The computed integral cross sections on the KPK surface are significantly closer to the experimental results than those obtained on the EG1 surface and are slightly better than the SAI1 results. The relaxation rates of the $j=19$ level at 450 K computed on the KPK, SAI1, and EG1 surfaces are too high relative to the experimental data by 55%, 76%, and 83%, respectively. The deviation from the experimental result is therefore least for the KPK surface.

The ^{3}He–CO_2 differential cross section exhibits the same amplitude as the ^{4}He–CO_2 system but the angular separation between consecutive minima is increased by 0.5° to 1.0°. This is consistent with the increased de Broglie wavelength for the ^{3}He system. Consequently, there is little additional information content in this isotope effect.

V. DISCUSSION AND SUMMARY

In this paper, we have utilized the infinite-order sudden approximation to examine total differential and integral cross sections, state-to-state cross sections, and the relaxation rates of depleted levels in the CO_2–He and CO_2–^{3}He systems on six different potential-energy surfaces.

Among the surfaces investigated, the KPK surface, which has been obtained by empirical fitting of the measured total differential cross section,[9] gives results that are in closest agreement with experiment. For the total integral and differential cross sections, this agreement is excellent. For the relaxation rate of the $j=19$ level at 450 K, the result is better than that obtained on either the EG1 or SAI1 surface, but it is still 53% larger than the reported value.[14,15]

The EG1 and SAI1 surfaces yield very similar results. The *ab initio* SAI1 surface gives total integral cross sections and relaxation rates in better accord with experiment[16] than EG1, but the phasing of the resonance maxima in the differential cross section is slightly better for the EG1 surface. Generally, the results indicate that for closed-shell systems a reasonably good potential surface may be obtained by combining a van der Waals attractive term with a repulsive interaction computed by either an electron-gas procedure or a Gaussian-orbital SCF calculation. If further empirical fitting is to be done, the differential cross sections are very sensitive probes of the surface topography and probably should be the data of choice.

The total elastic, inelastic, and differential cross sections are very sensitive to the long-range attractive terms in the potential. This is particularly true at lower energies. Generally, the cross sections increase significantly as the attractive potential increases in magnitude. However, for very small potential wells, the opposite trend is seen due to a partial cancellation of attractive and repulsive forces.

In contrast, the relaxation rates of a depleted j level are rather insensitive to the topographical details of the surface. In general, these rates are found to increase with both increasing temperature and decreasing reduced mass, due primarily to an increase in the collision frequency. The relaxation rate is found to be almost independent of the quantum number of the depleted level provided the other levels in the system remain unperturbed. Since the CO_2 moment of inertia does not enter the IOSA calculations, it may be inferred that this type of behavior will be observed in other systems for which the IOSA is applicable, i.e., for near "classical" systems with closely spaced rotational levels.

Except at very low energies, the total elastic and inelastic cross sections are found to decrease with increasing energy. Transitions associated with large Δj have appreciable cross sections and rate coefficients that decrease as Δj increases. However, because of an averaging effect, the total inelastic cross section out of state j is almost j independent.

The IOSA results are in excellent agreement with QCT calculations for the relaxation rate and total inelastic cross section. State-to-state transition rate coefficients and integral cross sections obtained from the IOSA are smaller than the QCT results for low values of the energy and for deexcitations associated with large Δj. For excitations with large Δj, this difference is reversed. This is not surprising since the IOSA equations are independent of the energy requirement for excitation of the rotor. This point leads to an increased error in the results as j' increases. In fact, some significant nonzero values have been obtained for $\sigma(j' \leftarrow j)$ for transitions that are closed by energy conservation constraints. For example, at $E_R = 0.0537$ eV, $\sigma(j' \leftarrow 19)$ must be zero

for $j' > 39$. However, one obtains 0.114 and 0.002 Å^2 for $j' = 45$ and 55, respectively, on the EG1 surface. Consequently, one might expect that $\sigma(j' \leftarrow j)$ is somewhat too large for transitions with large Δj and $j' > j$.

ACKNOWLEDGMENTS

The authors are pleased to acknowledge helpful discussions with Dr. Russell T Pack. We also thank Dr. Pack for providing us with some of his unpublished trajectory results. We would also like to thank Mrs. Rajalakshmi Viswanathan for help with various aspects of the problem and for numerous helpful discussions. We gratefully acknowledge the National Science Foundation for financial support on Grant NSF-CHE78-25563 and the Oklahoma State University College of Arts and Sciences for providing generous use of their computational facilities. P. M. A. would like to thank the Government of Rajasthan (India) for granting him leave to pursue this research.

[1]N. Sathyamurthy and L. M. Raff, J. Chem. Phys. **66**, 2191 (1977); **72**, 3163 (1980).
[2]C. L. Stroud and L. M. Raff, J. Chem. Phys. **72**, 5479 (1980).
[3]For recent reviews see (a) M. Faubel and J. P. Toennies, Adv. At. Mol. Phys. **13**, 229 (1977); (b) J. D. Lambert, *Vibrational and Rotational Relaxation in Gases* (Clarendon, Oxford, 1977); (c) J. P. Toennies, Annu. Rev. Phys. Chem. **27**, 225 (1976); (d) W. A. Lester, Jr., Adv. Quantum Chem. **9**, 199 (1975); (e) G. G. Balin-Kurti, Int. Rev. Sci. Phys. Chem. Ser. 2 **1**, 285 (1975); (f) H. Rabitz, Annu. Rev. Phys. Chem. **25**, 155 (1974); (g) W. A. Lester, Jr., Methods Comp. Phys. **10**, 211 (1971).
[4](a) Walter Eastes and J. P. Toennies, J. Chem. Phys. **70**, 1644 (1979); (b) G. D. Barg, G. M. Kendall, and J. P. Toennies, Chem. Phys. **16**, 243 (1976).
[5]R. N. Porter and L. M. Raff, in *Dynamics of Molecular Collisions*, edited by W. H. Miller (Plenum, New York, 1976), Part B, pp. 1–52.
[6]G. A. Parker and R. T Pack, J. Chem. Phys. **68**, 1585 (1978).
[7]P. K. Cheo, Lasers **3**, 111 (1971).
[8]A. Lecuyer, J. Phys. (Paris) **36**, 617 (1975).
[9]M. Keil, G. A. Parker, and A. Kuppermann, Chem. Phys. Lett. **59**, 443 (1978).
[10](a) R. T Pack, J. Chem. Phys. **70**, 3424 (1979); **66**, 1557 (1977), and references therein; (b) R. Goldflam, D. J. Kouri, R. K. Preston, and R. T Pack, J. Chem. Phys. **66**, 2574 (1977).
[11]R. K. Preston and R. T Pack, J. Chem. Phys. **69**, 2823 (1978).
[12]G. A. Parker, R. L. Snow, and R. T Pack, J. Chem. Phys. **64**, 1668 (1976).
[13]R. T Pack, J. Chem. Phys. **64**, 1659 (1976).
[14](a) R. R. Jacobs, K. J. Pettipiece, and S. J. Thomas, Appl. Phys. Lett. **24**, 375 (1974); (b) R. R. Jacobs, S. J. Thomas, and K. J. Pettipiece, IEEE J. Quantum Electron. **10**, 480 (1974).
[15]R. L. Abrams and P. K. Cheo, Appl. Phys. Lett. **15**, 177 (1969).
[16]H. P. Butz, R. Feltgen, H. Pauly, and H. Vehmeyer, Z. Phys. **247**, 70 (1971).
[17](a) A. E. Loiko, B. A. Ivakin, and P. E. Suetin, Zh. Tekh. Fiz. **44**, 682 (1974) [English translation: Sov. Phys. Tech. Phys. **19**, 434 (1974)]; (b) J. Kestin and S. T. Ro, Ber. Bunsenges Phys. Chem. **78**, 20 (1974); (c) K. R. Harris, T. N. Bell, and P. Dunlop, Can. J. Chem. **50**, 1874 (1972); (d) I. Nagata and T. Hasegawa, J. Chem. Eng. Jpn. **3**, 143 (1970); (e) A. G. Karpushin and N. D. Kosov, Fizika (Alam-Ata) **1**, 127 (1970); (f) N. D. Kosov and A. F. Bogatyrev, Teplofiz. (Massoperenos) **7**, 497 (1968); (g) R. DiPippo, J. Kestin, and K. Oguchi, J. Chem. Phys. **46**, 4758 (1967); (h) B. A. Ivakin and P. E. Suetin, Zh. Tech. Fiz. **34**, 1115 (1964) [English translation: Sov. Phys. Tech. Phys. **9**, 866 (1964)].
[18]R. T Pack, Chem. Phys. Lett. **55**, 197 (1978).
[19]R. T Pack, J. Chem. Phys. **60**, 633 (1974).
[20]B. R. Johnson, J. Comput. Phys. **13**, 445 (1973).
[21]L. Eno and H. Rabitz, J. Chem. Phys. **72**, 2314 (1980).
[22]C. Stroud, Ph. D. Thesis, Oklahoma State University, Stillwater, Oklahoma (1978).
[23]H. H. Suzukawa, Jr., M. Wolfsberg, and D. L. Thompson, J. Chem. Phys. **68**, 455 (1978).